

Received July 29, 2019, accepted August 23, 2019, date of publication August 30, 2019, date of current version September 13, 2019.

Digital Object Identifier 10.1109/ACCESS.2019.2938522

Analyzing Visible Light Communication Through Air–Water Interface

MD SHAFIQL ISLAM¹ AND MOHAMED F. YOUNIS

Department of Computer Science and Electrical Engineering, University of Maryland, Baltimore County, Baltimore, MD 21250, USA

Corresponding author: Md Shafiqul Islam (mdislam1@umbc.edu)

This work was supported in part by the National Science Foundation, USA, under Contract 000010465.

ABSTRACT In underwater wireless networks (UWNs), conventionally there is no direct communication between an underwater node and a remote command center. A floating base-station is often used to serve as an interface to a UWN; such a base-station would typically have both acoustic and radio modems to communicate with underwater nodes and off-shore centers, respectively. Although employing an airborne base-station would avoid the logistically-complicated surface nodes deployment, communication across the air-water interface becomes the main challenge since it involves two mediums. This paper promotes a novel way to interconnect UWNs to airborne base-stations through visible light communication (VLC) links. The paper analyzes the viability of VLC across the air-water interface by determining the coverage area and intensity inside the water for a light transmitter placed in the air. We show that enough intensity can be achieved for VLC communication even in the presence of a wavy water surface. We then provide guidelines for using single and multiple light sources to establish robust VLC links under rough environmental conditions like high water current and turbidity. Our approach is validated using simulation and a lab experiment is done to validate the simulation result for flat water surfaces.

INDEX TERMS Air-water interface, free space optics, optical communication, underwater wireless networks, visible light communication.

I. INTRODUCTION

Underwater wireless networks (UWNs) are deemed promising technology with numerous applications such as marine biology, oil field monitoring, water pollution studies, security surveillance, naval combat, etc. In fact, about 70% of the earth is covered by water. Due to the high absorption and attenuation coefficient of radio waves in underwater environments, acoustics has been the prime choice for communication in the water medium [1]. However, an acoustic signal mostly attenuates when crossing the water surface and a UWN cannot be directly accessed from a ground station using acoustic links. Therefore, a typical UWN uses floating nodes, e.g., boats or buoys, which act as gateways. A gateway carries dual modems, an acoustic modem to communicate with underwater nodes and a radio modem to interact with command centers. Nonetheless, such an approach requires preplanning and is costly; in fact, it may be impractical in risky application scenarios, e.g., during combat, and too slow when dealing with emerging events. For example, when

monitoring an evolving event such as oil leakage or conducting search-and-rescue missions, sending a boat or anchoring a buoy, is logistically complicated and lacks responsiveness. Moreover, in military applications, a surface node can be easily detected and the presence of UWN may get uncovered. Therefore, an alternative means for reaching the UWN is needed.

This paper studies the viability of establishing a communication link across the air-water medium without the need for floating gateway nodes. As we already mentioned, radio and acoustic waves do not perform well across the water and air mediums. Another option could be using magnetic induction. However, the communication range using magnetic induction is very small and needs large antennas. In this paper, we promote the use of visible light, which can travel up to 100 meters in water depending on the quality of the water [2]. High bandwidth and low time latency make visible light more suitable for communication through the air-water interface. However, the shape of the water surface and water properties introduce some challenges. Depending on the wind, the water surface might be flat or wavy, which will dynamically vary the intensity and the area covered by a

¹The associate editor coordinating the review of this article and approving it for publication was Bora Onat.

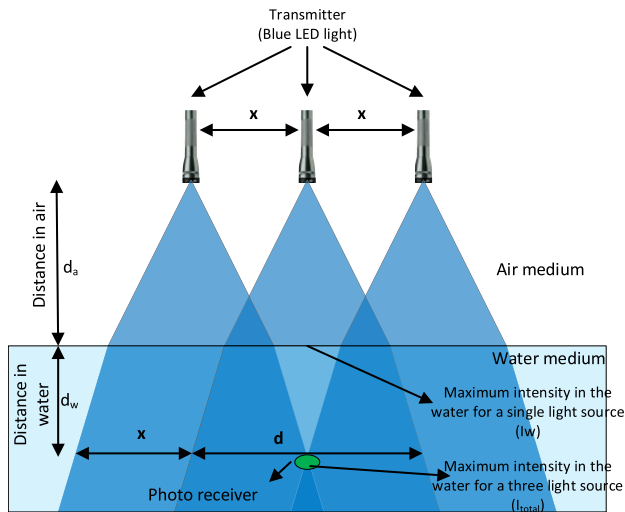


FIGURE 1. Communication through the air-water interface using multiple light sources.

light beam inside the water. The high water current could also cause an underwater node to drift away from the coverage area. Another important factor is that the attenuation coefficient of water, which increases in proportion to the water impurity level. Therefore, the communication system should be adaptive to handle various water properties. In this paper, we analytically study the effect of water surface and the various VLC parameters on the underwater coverage and optical beam intensity and provide guidelines for establishing robust VLC air-to-water links when using single and multiple light sources.

Figure 1 illustrates a visible light communication (VLC) system through the air-water interface. In this figure, three visible light sources have been placed in the air at d_a meter above the water surface. The target of our analysis is to measure the coverage area and intensity at d_w meter depth from the water surface. In the figure, the water surface is shown to be flat, but it could be wavy also. A single light source-based communication system provides better intensity and coverage in ideal conditions, i.e., when the water surface is flat. On the other hand, links based on beamforming multiple light sources perform well for a wavy surface and impure water. In [3], we have studied the coverage area and intensity inside the water for the flat surface. In this paper, we handle the general case of a wavy water surface for both single and beamforming multiple light sources. Thus, the contributions of this paper are: (1) studying the effect of air-water interface on underwater coverage and beam intensity for VLC, (2) analyzing the effect of water wave amplitude, wave period on coverage area, (3) determining the optical beam angle and underwater node position for best received signal strength, (4) developing a scheme for extending the coverage area by beamforming of multiple light sources, and (5) developing an algorithm to get the coverage area under rough water surface conditions. Both simulation and lab experiment are performed to validate the analytical results.

This paper is organized as follows. In section II, related work is discussed. Section III provides a system model. Communication across air-water interface using single and multiple light sources have been discussed in section IV and V, respectively. Section VI presents the validation results. The paper is concluded in Section VII.

II. RELATED WORK

In this paper, our focus is on analyzing suitable means for communication across the air-water interface. Acoustic waves are the prime choice for wireless communication in an underwater environment [4], [5]. However, acoustic waves suffer high attenuation in the air medium. On the other hand, the electromagnetic wave (EM) is broadly used to communicate in the air, yet it is not suitable for a water medium due to its high attenuation coefficient [6], [7]. Thus, neither EM nor acoustic waves can be used alone as a means for communication through the air-water interface. Another option could be magnetic induction (MI) as the magnetic permeability of air and water is almost the same, which helps MI for a smooth transition across the air-water interface [8]. Nonetheless, the conductive nature of the seawater affects the path loss and consequently makes the communication range very small. As shown in [9], the communication range of MI is limited to 4.5 meters. Visible light, on the other hand, performs moderately in both air and water medium in terms of communication range. To our best knowledge, no prior research work has studied the visible light as a means for communication medium through the air-water interface. It is only used in either underwater [10]–[12] or air (indoor environment) [13], [14].

In the literature, very few studies have targeted communication across the air-water interface. In [15], translational acoustic-RF communication (TARF) has been proposed. TARF supports only uplinks where data from underwater nodes are sent. The idea is that acoustic transmissions act as pressure waves that cause slight displacement upon striking the water surface. An airborne radar would measure these surface displacements and reform the acoustic wave. Not only TARF involves a very complex process, but also little details are provided for how the displacement in the water surface can be differentiated from the natural surface vibration and on how data could be modulated and encoded. On the other hand, the optoacoustic effect is exploited for the downlink [16], [17]. However, opto-acoustic energy transfer is a complex process and the bandwidth is limited by the underwater acoustic channel which is much less than the optical channel.

In order to communicate through the air-water interface, the wavy water surface will increase scattering. Only a few publications have considered the effect of a wavy water surface. Peng *et al.* [18] have designed an adaptive filter to suppress the interference caused by the water waves to detect opto-acoustic conversion more precisely. In [19] the authors characterize the behavior of the optical link under various conditions like in air-water interface, still water, and turbid

water. To mitigate turbulence-induced fading, spatial diversity has been pursued in [20]. However, no published research work has comprehensively studied the effect of water surface properties like wave amplitude and wave frequency. This paper fills such a gap and studies the intensity and coverage area in underwater for VLC system.

III. SYSTEM MODEL

In order to communicate through the air-water interface using optics we first discuss what type of optical signal is most suited for this task and provide a details analysis of water surface. In this section, we highlight the different types of optical signals and how we can model the water surface based on shallow and deep water.

A. BEST SUITED OPTICAL SIGNAL

In Section I, we have discussed why the optical signal is the best one to communicate through the air-water medium. There are two types of optical signals which are mainly used in wireless optical communication, namely laser and visible light. Due to the high directivity of the laser light, it can penetrate the water surface much more than visible light [21], [22]. However, such high directionality also complicates the establishment of communication links since it is hard to precisely target an inherently moving underwater receiver, e.g., due to water current. On the other hand, visible light with limited beam angle could provide reasonable penetration and coverage at the same time. Directional high-power Light-emitting diode (LED) has been improved a lot in recent years and made visible light communication a viable option. Moreover, secondary optics like lenses, reflectors, TIR (total internal reflection) optics, etc., can help in collimating the light rays to increase the light intensity. For example, the WAYLLSHINE® Zoomable Yard Flashlight [23] has a built-in lens that changes the beam angle of light, which ultimately controls the area of the spotlight. Moreover, among the visible light sources, blue and green light attenuates least in the water environment [24], [25]. So, in our experiment, we have used blue LED light sources.

B. MODELING THE WATER SURFACE

The water surface is not typically flat, where there is often a wave in air-water interface due to the wind. It is very difficult to find an exact equation for the surface wave. In general, the surface wave mainly depends on water depth and wind speed. Figure 2 shows a simple water surface function and associated parameter. Here the surface elevation is a cnoidal wave. As seen in the figure, a cnoidal wave has a higher crest and a flatter trough than a sine wave. If h is the water depth and λ is the wavelength of the water surface wave, then in shallow water $\lambda > h$. For shallow water, Boussinesq equations and Korteweg–de Vries equation (KdV) is the popular mathematical model for the water surface [26]. The solution of KdV is a cnoidal wave whose shape looks like the one that has been shown in Figure 2. The cnoidal-wave solution of the

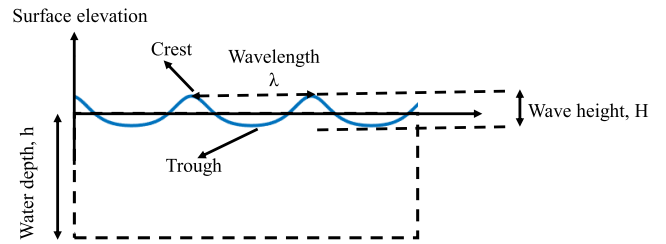


FIGURE 2. Illustrating the shape of a cnoidal wave.

KdV equation can be presented as follows [27]:

$$\eta(x, t) = \eta_2 + H.J^2 \left(\frac{x - c.t}{\Delta} | m \right), \quad (1)$$

where η = surface elevation, x = horizontal coordinate, t = time, H = wave height, η_2 = trough elevation, c = phase speed and J is one of the Jacobi elliptic functions. η_2 , Δ , λ , and c can be expressed as follows:

$$\eta_2 = \frac{H}{m} \left(1 - m - \frac{E(m)}{K(m)} \right), \quad \Delta = \frac{\lambda}{2.K(m)} = h\sqrt{\frac{4.m.h}{3.H}}, \quad (2)$$

$$c = \sqrt{g.h} \left[1 + \frac{H}{m.h} \left(1 - \frac{1}{2}m - \frac{3}{2} \frac{E(m)}{K(m)} \right) \right] \text{ and } \tau = \frac{\lambda}{c}. \quad (3)$$

On the other hand, general waves governed by Stokes' wave theory apply for intermediate and deep water [28]. Deep water is characterized with water depth that is much larger than wavelength ($h > \lambda$). According to Stokes' third-order theory, the water surface elevation can be expressed as follows [29]:

$$\eta(x, t) = \alpha \left\{ \left[1 - \frac{1}{16} (k.\alpha)^2 \right] \cos \theta + \frac{1}{2} (k.\alpha) \cos 2\theta + \frac{3}{8} (k.\alpha)^2 \cos 3\theta \right\} + \mathcal{O}((k.\alpha)^4), \quad (4)$$

$$c = \frac{w}{k} = \left(1 + \frac{1}{2} (k.\alpha)^2 \right) \sqrt{\frac{g}{k}} + \mathcal{O}((k.\alpha)^4),$$

$$\theta(x, t) = kx - wt, \quad k = \frac{2\pi}{\lambda}, \text{ and} \quad (5)$$

$$H = 2\alpha \left\{ 1 + \frac{3}{8} (k.\alpha)^2 \right\}, \quad (6)$$

where $k.\alpha$ is the wave steepness. If the value of $k.\alpha$ is larger in Figure 2, the crest will be steeper, and the trough will be flatter. The solution of eq. (4) is also a cnoidal type. In the analysis below, we will denote a water surface wave with $\eta(x, t)$, and depending on the water depth we use either eq. (1) or eq. (4), where for flat surface we will put simply $\eta = 0$. In the next section, we will show how these water surface models are used to enable communication across the air-water interface either using single or beam-formed multiple light sources.

TABLE 1. A summary of the important notations.

Notation	Description
θ	Beam angle of light source
d_a	Proximity of the light source to the surface
d_w	Depth at which the underwater node exists
θ_i	Incident angle of light on the water surface
φ_i	Refraction angle of the light beam
φ	Angle of the refracted light beam edge
d	Diameter of the coverage area
η	Reflectance of light
τ	Transmittance of light
P	Power of single light source

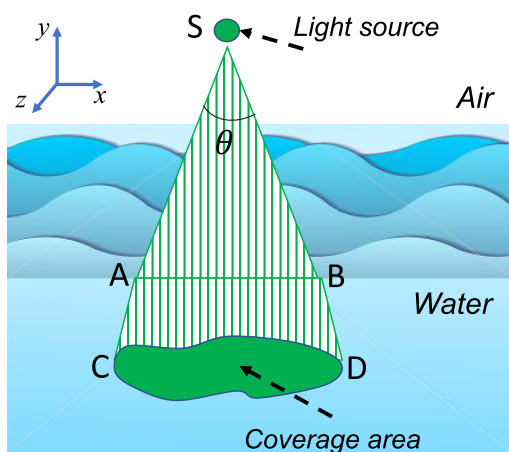


FIGURE 3. 3D view of a coverage area inside the water.

IV. VLC COMMUNICATION USING A SINGLE LIGHT SOURCE

In this subsection, we analyze how we can use a single light source to communicate through the air-water interface. For this purpose, we will place a light source at a specific height from the water surface and focus the light into the water. Then we will analyze the intensity of light at a specific underwater depth. We use a light source with an adjustable beam angle so that we can control the intensity and coverage area inside the water. Table 1 provides a summary of the parameters used in the analysis. Here, we assume that the water medium is homogeneous. In our work, we refer to the spotlight inside the water as the coverage area.

Figure 3 shows the 3D view of a single light transmitter S and the corresponding underwater coverage area. As seen in the figure, a light beam gets refracted as it penetrates the water surface. For a flat water surface the coverage area inside the water will be circular but if the water surface is wavy the coverage area will be irregularly shaped as shown in Figure 3. Basically, the conical propagation of the light will not be evenly refracted since the water surface is wavy. To determine the boundary of the coverage area, we first consider a cross section of the cone, e.g., the 2D plane of the two light

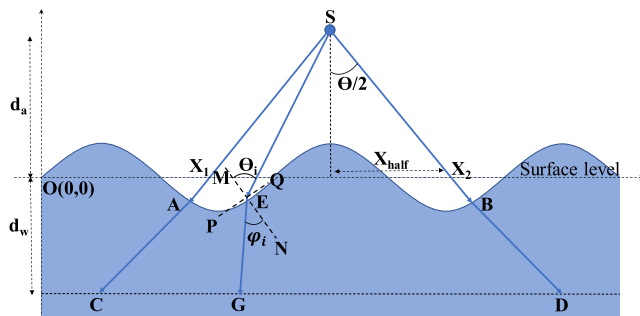


FIGURE 4. Illustration of light ray direction in a wavy surface.

beams SA and SB on the cone surface, and then determine the corresponding underwater point C and D on the boundary of the underwater coverage area. When rotating such a 2D plane, two more points on the coverage area boundary can be determined. By incrementally rotating the 2D plane up to 360° we can fully define the underwater coverage area, as we explain below.

A. SINGLE SOURCE ANALYSIS

Figure 4 shows a detailed view of the 2D plan used in the first step. The x -axis in Figure 4 is the water level in absence of any waves; the water surface disperses from this level to become wavy. The point $O(0,0)$ is considered the origin. A light source is placed at point $S(x_s, y_s)$ which is at a distance d_a meter above the water surface. θ is the beam angle of the light source. Ray SE is the incident ray from light source S , which strikes at point $E(x_e, y_e)$ on the water surface at incident angle θ_i with line MN . Here MN is the normal line of PQ , where PQ is the tangent at point E . The light ray gets refracted at point $G(x_g, y_g)$ from point E making the transmission angle φ_i . The coverage area will be determined by the refracted version of the boundary rays of the transmitted light beam. Moreover, to calculate the light intensity at an underwater point G , we need to determine the distance \overline{SE} and \overline{EG} , and angles θ_i and φ_i . The following shows how these measures are determined.

Assume that the water surface function is:

$$y = f(x). \tag{7}$$

For wavy water surface we can get the surface function using either eq. (1) or eq. (4) and for flat surface this is simply a straight line. The tangent at any point on the water surface is the first derivative of surface function on that point. Thus, the slope at point E is:

$$m_{PQ} = f'(x_e). \tag{8}$$

In order to calculate incident angle θ_i , we need to know the slope of SE and MN , which can be calculated as:

$$m_{SE} = \frac{y_s - y_e}{x_s - x_e} = \frac{y_s - f(x_e)}{x_s - x_e}, \tag{9}$$

$$m_{MN} = \frac{-1}{m_{PQ}} = \frac{-1}{f'(x_e)}. \tag{10}$$

Now, the angle between SE and MN is:

$$\tan \theta_i = \left| \frac{\frac{y_s - f(x_e)}{x_s - x_e} + \frac{1}{f'(x_e)}}{1 - \frac{y_s - f(x_e)}{(x_s - x_e)f'(x_e)}} \right|,$$

$$\rightarrow \theta_i = \tan^{-1} \left| \frac{f'(x_e)(y_s - f(x_e)) + (x_s - x_e)}{(x_s - x_e)f'(x_e) - y_s + f(x_e)} \right|. \quad (11)$$

If we know the incident angle, θ_i we can calculate transmission angle φ_i using Snell's law:

$$n_a \cdot \sin \theta_i = n_w \cdot \sin \varphi_i. \quad (12)$$

Hence, the slope of line EG is:

$$m_{EG} = \frac{y_g - f(x_e)}{x_g - x_e} \rightarrow x_g = x_e + \frac{y_g - f(x_e)}{m_{EG}}. \quad (13)$$

Now the relation between φ_i , m_{EG} and m_{MN} is:

$$\tan \varphi_i = \left| \frac{m_{MN} - m_{EG}}{1 + m_{MN} \cdot m_{EG}} \right|. \quad (14)$$

If we expand eq. (14) for m_{EG} then we get:

$$(m_{MN}^2 \cdot \tan^2 \varphi_i - 1) \cdot m_{EG}^2 + 2 \cdot m_{MN} (1 + \tan^2 \varphi_i) \cdot m_{EG} + \tan^2 \varphi_i - m_{MN}^2 = 0. \quad (15)$$

Eq. (15) is a quadratic equation of m_{EG} . By solving this equation, we will know the value of m_{EG} and substituting the value in eq. (13) we get x_g . The value of y_g is simply d_w . Hence, we know the point $G(x_g, y_g)$. We next show how to use the above analysis to estimate the coverage area and light intensity.

B. COVERAGE AREA

Based on the above analysis, for known water surface function and position of the light source, we can find the refracted ray in underwater at a given surface point. Figure 4 represents a simple case where lines SA and SB are two end rays in the air and the lines AC and BD are the corresponding refracted rays. Thus, if we know points A and B , in this case, we can determine points C and D , respectively, and the line CD contains all the points where the light goes after refraction. Remember this is just one cross-section of the coverage area. As illustrated in Figure 4, let X_1 and X_2 be the points where the lines SA and SB intersect with the x -axis, respectively. For a known beam angle, θ , the distance between the middle point of the line X_1X_2 and either point X_1 or X_2 can be calculated as follows:

$$X_{half} = d_a \tan \frac{\theta}{2}. \quad (16)$$

Now, we can easily calculate the position of point X_1 and X_2

$$X_1 \equiv (X_s - X_{half}, 0), \quad X_2 \equiv (X_s + X_{half}, 0). \quad (17)$$

The equation for line SX_1 (or SA) is:

$$\frac{x - x_s}{x_s - x_s + X_{half}} = \frac{y - y_s}{y_s - 0}$$

$$\rightarrow y_s \cdot x - X_{half} \cdot y - x_s \cdot y_s + X_{half} \cdot y_s = 0. \quad (18)$$

By solving eq. (18) we determine the coordinates of point A . This equation can only be solved numerically, e.g., by applying the Newton Raphson method. Let's assume initial solution of point A is x_0 then we can iterate and converge to the solution using: $x_{n+1} = x_n - \frac{f(x_n)}{f'(x_n)}$.

Similarly, we can determine the coordinates of point B . After calculating the coordinates of the two endpoints, namely, A , and B , we can determine points C , and D using equations (13) and (15). To extend the analysis to 3D, the same steps can be followed to determine the coordinates of all boundary points of the covered underwater area (i.e., a source with the same θ and relative position to the water surface, and the same surface function). This is like rotating the line X_1X_2 horizontally in the $x - z$ plane from 1° to 360° . The accuracy of the coverage boundary will depend on the radial angle increment. Figure 5 shows examples for such an area based on radial angle increment of 1° . We study the effect of the radial increment later in this section.

The analysis above implicitly assumes that the light source transmits when its position is vertically aligned with the peak of the sinusoidal surface function. However, in practice, such alignment is rare where the water wave always changes with time and consequently the coverage area will vary. Figure 5 shows such variation in the coverage area for both shallow and deep water at different times. The figure also shows the coverage area for the flat-water surface case. For both the shallow and deep-water cases coverage area is randomly changing over time. The variation is less significant for shallow water (Figure 5(a)) because of the high wavelength and relatively low amplitude of the water wave. Figure 5(b) shows the results for the deep-water scenario. In this figure, the coverage area varies significantly due to the low wavelength. Figure 5(c) shows the result of a flat-water scenario. From this figure, we can see there is no change in the coverage area over time which is very much expected for a flat non-varying surface.

It is worth reminding that our goal is to find the underwater area that consistently receives light. Finding such an area is very complex for wavy water surface; therefore, we approximate it using a circle that is centered at the projected position of the light source, and whose radius is the minimum distance from its center to the boundary of the coverage area for all possible phases. We call such a circle the effective coverage area. The dotted circle in Figure 5(a) and (b) reflects the effective coverage and corresponds to the area that gets light at all times. For a flat-water scenario, Figure 5(c) confirms that effective coverage area and coverage area are the same. Note that in Figure 5 we show the coverage area on the $x - z$ plane, where the transmitter is placed in y -axis at a

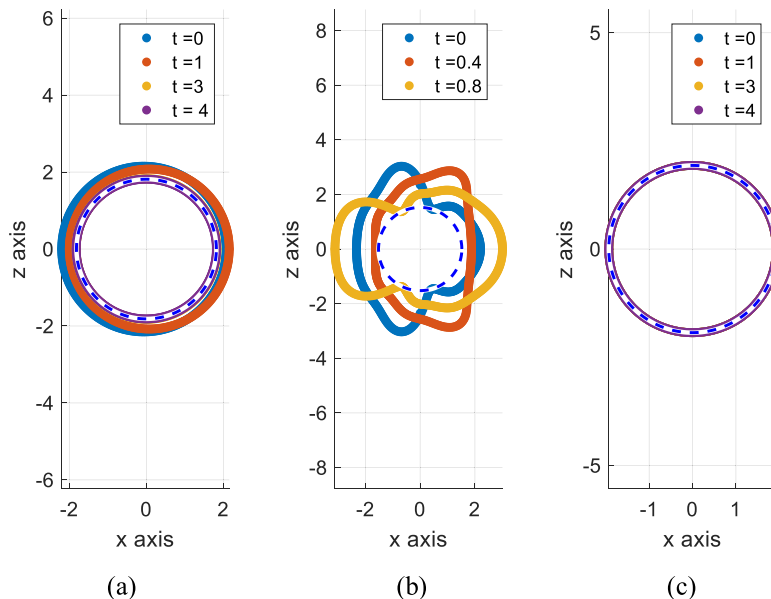


FIGURE 5. Illustrating the difference between the actual and effective coverage area for (a) shallow water ($H = 0.1$ meter, $T = 5.6$ sec, $\lambda = 30$ meters and $h = 3$ meters), (b) deep water ($H = 0.2$ meter, $k \cdot \alpha = 0.45$, $\lambda = 1.3$ meters $T = 1.2$ sec; $h = 10$ meters), and (c) flat water surface.

distance d_a meter above from the water surface level (see Figure 4). Thus, the position of the light source is $(0, d_a, 0)$.

Algorithm 1 Summary of the Steps for Defining the Effective Coverage Area

```

 $r_{eff} = 0$  // The effective radius  $r_{eff}$ 
for (time = 0 to  $T$ , step  $\Delta t$ .)
– Calculate all underwater point across line  $\overline{CD}$ 
– Rotate the axis according to  $\Delta r$  from  $0^\circ$  to  $360^\circ$  in order to determine the coverage area
–  $R =$  minimum distance of coverage area from the projected position of the light source
–  $r_{eff} = \min(r_{eff}, R)$ 
end for
    
```

1) ALGORITHM AND OPTIMIZATION

Algorithm 1 summarizes the steps for finding the effective coverage area. The algorithm iterates over full wave period, T , with an increment of Δt . For each of the considered wave, the coverage area is determined using a cross section (2D plane) and then rotating it from 0° to 360° with an increment of Δr . The value of Δr simply determines how accurate (continuity) is the coverage area boundary. For each 2D plan, we calculate the proximity of the boundary points to the projected position of the light source and track the minimum value over all iterations. After considering all times from 0 to T , the minimum distance becomes the radius of the effective coverage area (r_{eff}). The runtime complexity of Algorithm 1 is $O(\Delta r \cdot \Delta t)$. As mentioned above, the values of Δr vary from 0° to 360° and Δt vary from 0 to T , where T is the period of the water wave function.

For example, if $\Delta r = 1$, $\Delta t = .1$ and $T = 5$ sec, eq. (44) will be solved $360 \times 50 = 18,000$ times. Obviously, there is a tradeoff where a higher accuracy for determining the coverage area, requires increased computational overhead.

Nonetheless, major optimization can be made if the frequency of the water wave is reasonably high (small period and wavelength), such that the light transmission, i.e., width of the cone base, covers one full cycle of the water wave. Basically, in such a case if Δr is small enough the value of r_{eff} does not change for the various time phases because r_{eff} corresponds to a specific wave amplitude and incident angle. Thus, in this particular case the light propagation experiences the same wave amplitude and incident angle for all times within T and consequently, we do not need to vary the time phases, i.e., we do not need to run the loop for Δt , which expedites the algorithm execution. It is worth noting that this particular case is expected in almost all practical scenarios; for example, if $d_a = 5$ meters, $d_w = 5$ meters, and $\theta = 50^\circ$ the coverage area is 40 m^2 which means the diameter of the coverage area is approximately 7 meters. The coverage area even grows with beam angle and underwater depth as shown in the next section. Figure 5(b) shows the simulation results to capture the effect of Δr when the light beam covers at least one full period of the water wave. As seen in the Figure, for each snapshot the circle touches the corresponding coverage area at least once. Accordingly, we only need to vary Δr to get the r_{eff} for a case where Δr is small enough and the transmitter beam angle θ is large enough so that the light covers at least one full cycle of the water surface wave. The effect of Δr on r_{eff} is highlighted in Figure 6, where increasing Δr causes a major decline in the runtime complexity and a slight decrease in accuracy. A setting of Δr up to a value of 5 will have

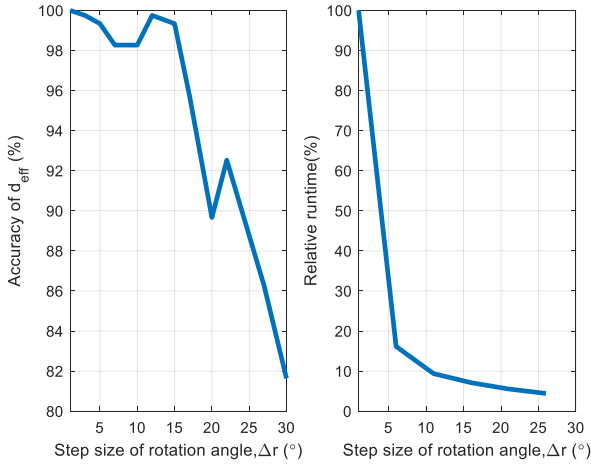


FIGURE 6. Effect of the rotation angle increment on accuracy of r_{eff} and runtime of the algorithm. Note that relative runtime means in comparison to the case where $\Delta r = 1$.

an unnoticeable impact on accuracy while dropping runtime by 27% relative to $\Delta r = 1$.

No optimization is required for a flat-water surface scenario because the algorithm needs to run only once to determine the coverage area.

C. LIGHT INTENSITY

In the air, if we know the distance that light travels, then it is very easy to find the intensity. Using the location of points S , E and G , in Figure 4, we can easily calculate the distance between them.

$$\overline{SE} = \sqrt{(x_e - x_s)^2 + (y_e - y_s)^2}, \tag{19}$$

$$\overline{EG} = \sqrt{(x_e - x_g)^2 + (y_e - y_g)^2}. \tag{20}$$

However, the light intensity at point G depends not only on the distance but also how much light is penetrating the surface to the water, i.e. we need to know the transmittance, τ and reflectance, η of the water surface. The relation between τ and η is:

$$\tau = 1 - \eta. \tag{21}$$

Now, the reflectance η depends on the incident and transmittance angle and polarity of the light source. If the light source is not polarized, then we can express reflectance as follows:

$$\eta = \frac{\eta_s + \eta_p}{2}, \tag{22}$$

where η_s and η_p are the reflectance coefficients of s -polarized light and p -polarized light, respectively. To determine η_s and η_p , Fresnel equation can be used. If n_a and n_w are the refractive indexes of air and water respectively, then using Fresnel equation η_s and η_p are:

$$\eta_s = \left| \frac{n_a \cos \theta_i - n_w \cos \varphi_i}{n_a \cos \theta_i + n_w \cos \varphi_i} \right|^2 \text{ and } \eta_p = \left| \frac{n_a \cos \varphi_i - n_w \cos \theta_i}{n_a \cos \varphi_i + n_w \cos \theta_i} \right|^2. \tag{23}$$

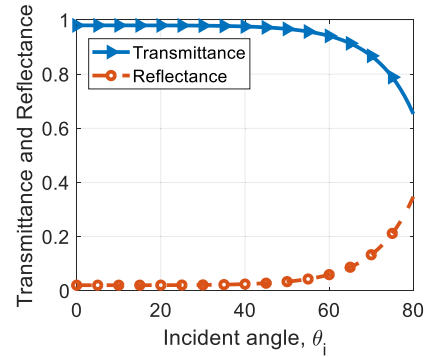


FIGURE 7. Relationship between transmittance and reflectance and the incident angle.

Using eq. (21), (22), and (23) we can show in Figure 7 the relationship between reflectance and transmittance and the incident angle. Figure 7 indicates for incident angle below 60° , the transmittance τ is almost one.

After measuring the distances and calculating transmittance, we find the intensity at point G in Figure 4. Let's assume, I_e is the intensity at point E which is just above the water surface and I_{ew} is the intensity just below the water surface at the same point. I_e and I_{ew} can be calculated as follows,

$$I_E = \frac{2\pi}{\theta} \cdot \frac{P}{4\pi \cdot SE^2}, \tag{24}$$

$$I_{ew} = \tau \cdot I_e, \tag{25}$$

where P is the power of the light source at point S . The intensity I_{ew} will decrease as light travels in the water depending on the beam attenuation coefficient, k (m^{-1}), of light in the water medium. Thus, the light intensity at point G after traveling \overline{EG} distance in water can be calculated using Beer's law as [20]:

$$I = I_{ew} \cdot e^{-k(EG)}. \tag{26}$$

Generally, the value of k depends on the biological factors of water and absorption, a (m^{-1}) and scattering, b (m^{-1}) coefficient. A details analysis of how we can calculate the value of k has been given in Appendix A. Eq. (26) is valid when no scattered light is recollected. However, some portion of the scattered light may reenter into the receiver FOV. In Appendix A, we have also shown how to calculate the recollection of the scattered light using eq. (38). In that calculation, a scattering factor n ($0 \leq n \leq 1$) is used to recollect scattered light. This scattering factor is a function of the water optical properties (i.e., absorption, scattering, and total attenuation) and system parameters (i.e., receiver polarization state, aperture, FOV, and initial laser beam radius and divergence). Figure 8 illustrates the effect of the scattering factor on light intensity. In this figure, the y -axis reflects the intensity at a specific depth of water relative to the intensity at the water surface. As shown in Figure 8, the intensity of the light grows with the increase of the scattering factor. In the figure, $n = 0$ corresponds to the case when no scattering light is collected. How to determine the absorption, scattering and

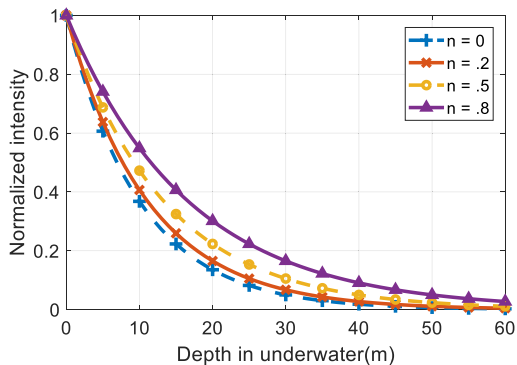


FIGURE 8. Effect of scattering factor, n on the light propagation.

scattering factors can be found in [30]–[32]. Assuming that the values of these factors are known, we will calculate the light intensity in underwater, e.g., at point G. Using eq. (24), (25) and (26), the light intensity at point G will be:

$$I = \frac{2\pi P}{4\pi\theta} \cdot \tau \cdot \frac{1}{SE^2} \cdot e^{-k \cdot (EG)}. \quad (27)$$

Eq. (27) provides the intensity at point G. If we know all points at the water surface, i.e. surface function, we can find the intensities at all points covered by the light sources at depth d_w .

1) INTENSITY FOR A FLAT SURFACE

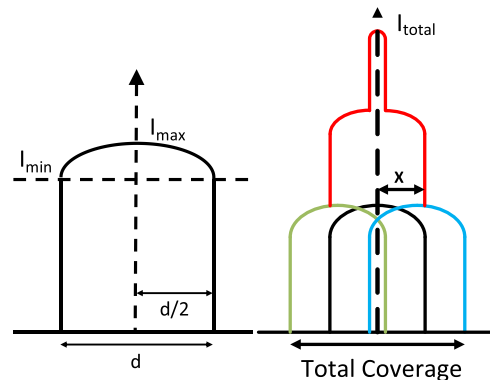
For a flat-water surface, eq. (27) can be simplified. When incident angle, θ_i is minimum, i.e. zero, the distances \overline{SE} and \overline{EG} become minimum, specifically, $\overline{SE} = d_a$ and $\overline{EG} = d_w$. In this case, the intensity is maximum. Reflecting this condition in eq. (27) we can get the maximum intensity I_{max} for a flat-water surface as follows:

$$I_{max} = \frac{2\pi P}{4\pi\theta} \cdot \tau \cdot \frac{1}{d_a^2} \cdot e^{-k \cdot (d_w)}. \quad (28)$$

The minimum intensity, I_{min} , corresponds to $\theta_i = \theta/2$ and $\phi_i = \phi$. In this case \overline{SE} and \overline{EG} become maximum where $\overline{SE} = \frac{d_a}{\cos \frac{\theta}{2}}$ and $\overline{EG} = \frac{d_w}{\cos \phi}$. Reflecting this condition in eq. (27), I_{min} for flat water surface will be:

$$I_{min} = \frac{2\pi P}{4\pi\theta} \cdot \tau \cdot \frac{1}{\left(\frac{d_a}{\cos \frac{\theta}{2}}\right)^2} \cdot e^{-k \cdot \left(\frac{d_w}{\cos \phi}\right)}. \quad (29)$$

Using Algorithm 1 we can find the coverage area and using eq. (27), (28), and (29) we can calculate the intensity on that area. Figure 9(a) shows such theoretical relation between coverage area and intensity for a flat-water surface, where d is the diameter of the coverage area. From this figure we can see, the light is confined within a circle with diameter d for a specific beam angle, θ . The intensity is zero outside, maximum (I_{max}) in the middle (center) and minimum in the edges (I_{min}) of this circular area. By controlling θ , d_a , d_w , and P , the value of d , I_{max} , and I_{min} can be varied. In the next section, we leverage the above analysis of a single light source to study the cases of multiple beamformed light sources.



(a) Single light source (b) Three light sources

FIGURE 9. Relation between coverage area and intensity for single light source and three light sources.

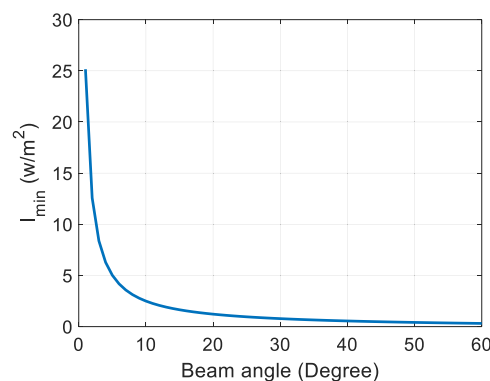


FIGURE 10. Changes of I_{min} for different beam angles of a single light source. The plot is based on setting $d_a = 10m$, $d_w = 10m$ and $\rho = 100w/m^2$.

V. USING MULTIPLE BEAMFORMED LIGHT SOURCES

In the previous section, as we analyzed the underwater coverage and intensity for a single light source. The coverage area inside the water mainly depends on the light source beam angle, θ , and grows with the increase of θ . On the other hand, the light intensity within the covered underwater area depends on both light source power, P and θ . If P is constant, the light intensity diminishes with the increase of θ . We are particularly interested in I_{min} because it reflects the ability of an optical receiver to successfully receive a transmission. Using eq. (29) we can determine the relation between I_{min} and θ , which has been shown in Figure 10. From this figure, it is obvious that I_{min} decreases quickly when broadening the angle θ . On the other hand, having a large coverage area is also an important factor for successful transmission because of the uncertainty of the underwater node position due to the water current. Thus, there is a tradeoff between coverage area and intensity.

Through our analysis in this section, and also the simulation results in Section VI, we will show how we can get the better gain in the coverage area and intensity using the same total transmission power distributed into multiple light sources, as illustrated in Figure 1. We call it beamforming multiple light sources. In optical beamforming, the coverage area of multiple light sources overlaps inside the water and

the light intensity on that region becomes the sum of that the individual light sources. Maintaining higher coverage area using optical beamforming has some other advantages as well. In [33], a secure downlink transmission communication link has been made using multiple light inputs by designing transmit beamformers that maximize the achievable secrecy rate. Moreover, a higher signal-to-interference-plus-noise ratio (SINR) is possible using beamforming. In [34] a multi-element VLC transmitter architecture for different configurations is proposed. Multi-element transmitters with three, seven, and nineteen light emitting diodes (LEDs) are compared with a single light transmitter in terms of SINR and illumination. The transmitter configuration with three LED has been found to yield the best performance for simultaneously achieving good illumination and SINR distribution.

A. POSITIONING OF MULTIPLE LIGHT SOURCES

Based on the analysis in the previous section for a single light source, here we study the positioning of multiple beamformed light sources so that the size of coverage area is maximized while keeping the intensity level throughout the covered area sufficiently high for good SINR. We distribute the same power P which is used for the baseline setup of a single light source, among the beamformed transmitters. For example, if we have four beamformed sources, each is allocated power of $P/4$. It should be noted that if there is no power budget, i.e., one can use the same power P for all transmitters, the positioning problem becomes finding coverage patterns with least overlaps, which has been extensively used in the realm of sensor networks [35]; with the constrained total power budget, the problem becomes more complicated due to the coverage and intensity tradeoff as discussed at the beginning of this subsection. Thus, we opt to find the best number of beamformed transmitters and determine their positions relative to one another, i.e., deployment pattern.

Conventional node placement for maximized coverage opts to employ the least number of nodes; thus, the objective is to minimize overlap among the regions covered by the individual nodes. Fundamentally a placement pattern is determined, and the entire deployment area is then tiled using such a pattern. In the realm of sensor networks, an equilateral triangle has been shown to achieve optimal results, where sensors of disc-shaped ranges are placed on the vertices of the triangles [35]. In such a pattern, there is no point in the triangle that is covered by more than 2 sensors. However, for distributed beamforming, the placement pattern of the light sources should ensure the presence of a commonly covered region, i.e., a region that is covered by multiple beamformed sources, in order to enable the establishment of highly reliable communication links for the underwater receiver located in such a region. Figure 11 shows sample beamforming patterns for varying count and positions of light sources. As seen in the figure, the intensity in areas with non-overlapped coverage, i.e., I_{min} , diminishes with the increased number of sources, which ultimately leads to weaker SINR. Thus, it is important to have areas with maximal overlap among the sources.

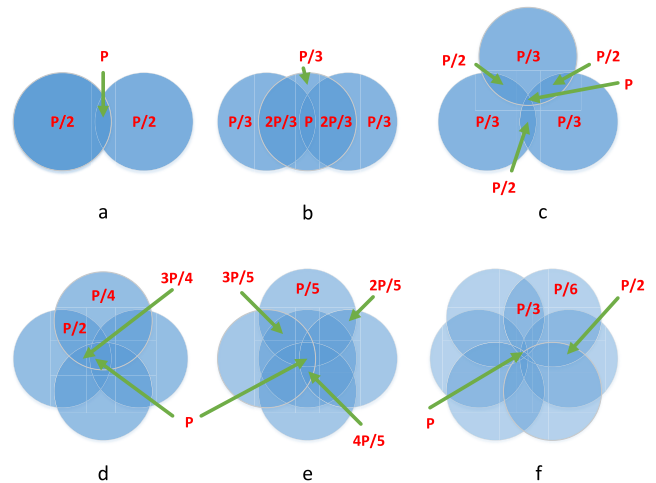


FIGURE 11. Sample arrangement for: (a) two, (b) three in straight line, (c) three in triangular, (d) four, (e) five, and (f) six light sources. Same power ' P ' is equally split among all sources.

Another important factor is the size of maximal coverage for the placement pattern; this is important to mitigate uncertainty about the location of the underwater nodes where water current causes the node to drift while communicating with the beamformed sources and between consecutive data sharing sessions with the airborne unit(s). Based on such a criterion, the placement pattern in Figure 11(b) is better than that in Figure 11(c) for three beamformed sources, despite the fact that the pattern of Figure 11(c) yields better coverage. Fundamentally, the pattern in Figure 11(b) has two advantages in our particular application. Firstly, as water current can cause an underwater receiver to drift away in one direction, the three light sources can be easily aligned in that direction. Secondly, due to the increased overlap in the central region, we can use that region for establishing a highly robust communication link between the airborne unit and the underwater node, i.e., we have a larger area that experiences I_{max} . With the increased number of light sources, it becomes quite difficult and inflexible to reposition the individual sources to cope with underwater drifts; especially the coverage area becomes more diverse in terms of the number of overlapped light sources. Furthermore, the splitting of the total power on many sources will diminish I_{min} and thus the increased coverage could more or less become illusive in this case since the receiver will experience low SINR in areas covered by few sources. For example, in Figure 11(f) areas covered only by one source will experience I_{min} that is $1/2$ that of those covered by one source in Figures 11(b) and 11(c).

B. ANALYSIS OF THREE BEAMFORMED LIGHT SOURCES

As concluded above, the collinear positioning of three light sources, shown in Figure 11(b), is deemed the most suitable arrangement for beamformed transmission across the air-water interface. This subsection analyzes the effect of the inter-source proximity on the coverage and light intensity for both flat and wavy water surfaces.

TABLE 2. Relation between total coverage and inter light source distance.

Distance (x)	Total coverage (C)
$d/2$	$3\pi\left(\frac{d}{2}\right)^2 - d^2 \cos^{-1}\left(\frac{1}{2}\right) + \frac{\sqrt{3}}{4}d^2$
0	$\pi\left(\frac{d}{2}\right)^2$
$0 < x < d/2$	$\pi\left(\frac{d}{2}\right)^2 < C < 3\pi\left(\frac{d}{2}\right)^2 - d^2 \cos^{-1}\left(\frac{1}{2}\right) + \frac{\sqrt{3}}{4}d^2$

1) FLAT WATER SURFACE

From Figure 1, the distance between two light sources is denoted by x , and the diameter of the coverage area of a single light source is referred to by d . We can calculate the total coverage area, C at d_w meter depth for three collinear light sources as follows:

$$C = 3\pi\left(\frac{d}{2}\right)^2 - d^2 \cos^{-1}\left(\frac{d-x}{d}\right) + (d-x)\sqrt{d^2 - (d-x)^2}. \quad (30)$$

The light intensity at any point within the C is the sum of the light intensity of individual light sources. If the intensity at any point at d_w meter depth for three light sources are I_1, I_2 , and I_3 , respectively, then Total intensity, I_{total} on that point is:

$$I_{total} = I_1 + I_2 + I_3. \quad (31)$$

Using eq. (30) we can calculate the coverage area for different inter-light sources distances, as shown in Table 2. We will study the coverage area and light intensity on that area more through simulation in the next section.

2) WAVY WATER SURFACE

Using Algorithm 1, we can find the effective diameter of the coverage area for a single light source. Let’s assume for some given parameter the diameter of the effective coverage area is d_{eff} and again if the distances between light sources are Δ meters, then we can get the coverage area for three light sources using eq. (30) as:

$$C_{eff} = 3\pi\left(\frac{d_{eff}}{2}\right)^2 - d_{eff}^2 \cos^{-1}\left(\frac{d_{eff}-x}{d_{eff}}\right) + (d_{eff}-\Delta)\sqrt{d_{eff}^2 - (d_{eff}-\Delta)^2}. \quad (32)$$

The value of d_{eff} depends on the water wave amplitude and frequency hence C_{eff} also depends on the water surface function. In the next section, we will study eq. (32) through simulation. For intensity calculation again if we know the intensity at a specific point for every single light source then the total intensity is simply the sum of all those intensities like eq. (31).

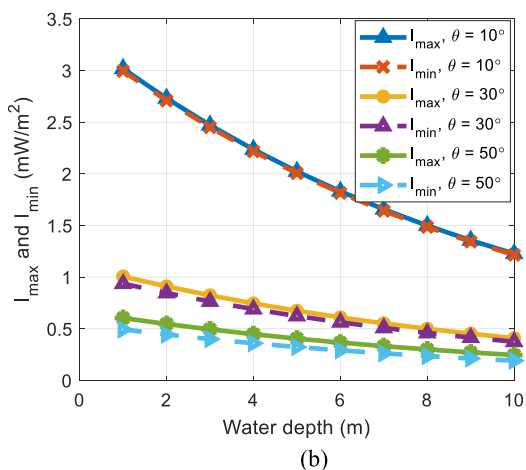
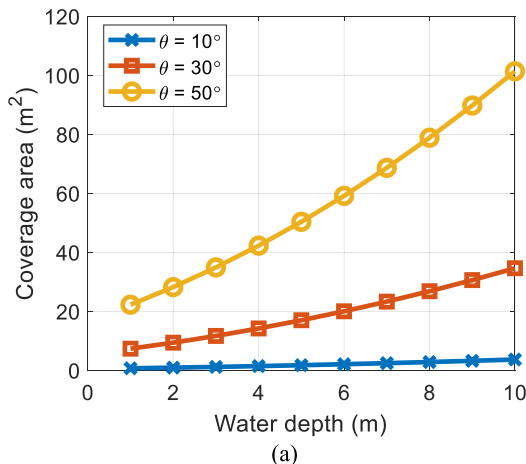


FIGURE 12. The coverage and light intensity at various underwater depth for a single light source placed in air at a height, $d_a = 5$ m, from the water surface with beam angle, $\theta = 10^\circ, 20^\circ$, and 50° .

VI. VALIDATION AND RESULTS

In this section, the coverage area and light intensity inside the water is extensively studied using MATLAB. The simulation is done for various surface wave parameters, beam angle, θ and for various values of d_a and d_w . In addition, a lab experiment has been conducted to validate the simulation results for flat water surface. Simulation is done for both wavy and flat surface. We will start with the flat surface simulation and then show the result for a wavy surface.

A. SIMULATION FOR A FLAT WATER SURFACE

The intensity and coverage area calculation are quite different depending on the surface function (flat or wavy). In this subsection, we present the results for a flat-water surface for both single and multiple beamformed light sources.

1) SINGLE LIGHT SOURCE

The effect of θ and d_w on the light intensity and coverage have been captured first for a single light source. Again, keep in mind that the coverage area is measured by tracking the diameter d of the coverage area for a single light source, i.e., $d = \overline{CD}$ in Figure 3. In this simulation, the transmitted

power, P is set to 30 mW and attenuation coefficient of water, $k = 0.1$ ($a = .05$, $b = 0.05$), $n = 0$ (no scattered light is collected). Moreover, we assume that transmittance, τ is constant and equals to 0.97 for all incident angles less than 60° , as explained in Figure 7. The value of d_w has been varied from 1 to 10 meters to track down intensity and coverage area while keeping d_a fixed for different θ ($\theta = 10^\circ$, 30° , and 50°). The results are plotted in Figures 12(a) and 12(b).

Figure 12(a) shows the relation between the size of the coverage area and water depth for various θ . The results indicate that θ has a dramatic effect on coverage. For small values of θ , the coverage area is very small which is risky since the underwater node may drift away from that small coverage area due to the water current. A large value of θ clearly gives better coverage, particularly for increased water depth. On the other hand, Figure 12(b) shows the relationship between I_{min} and I_{max} with θ and d_w . As expected, the light intensity is higher for smaller beam angles. The intensity diminishes rapidly for larger beam angle, especially the gap between I_{min} and I_{max} grows with the increased value of θ . Overall, the plot confirms the tradeoff between coverage and intensity which has been discussed in the previous section.

2) BEAMFORMED SOURCES

Figure 13 shows the same analysis for the multiple light sources. Here all parameter has been set exactly the same as the single light source except the total power P , where the total 30 mW has been divided equally among the three light sources. The inter-distance x between light sources has been set to $\frac{d}{2}$. Figure 13(a) and 13(b) shows the results for coverage and light intensity. When comparing Figure 12(a) and 13(a), it is obvious that beamforming multiple light sources almost doubles the coverage area for the same θ and d_w . It is very important for tolerating node drifts and thus enabling the establishment of robust communication links. Figure 13(b) shows the result of light intensity. The figure shows that beamforming does not affect the I_{max} , yet I_{min} is significantly less than the Figure 12(b), which is very much expected since the transmission power of each of the three sources is 1/3 that of the single source used for Figure 13(b). In practice, I_{min} is very important and determines the number of sources and the total power since it affects the SINR.

Figure 14 opts to highlight the trade-off between the coverage area and light intensity for various transmitter positioning options involving a single and multiple light sources. In this simulation, we have placed light transmitters in the air to generate the pattern of coverage area inside the water shown in Figure 11. In Figure 14(a), the light intensity is shown (y-axis) while the x -axis represents the line along which intensity is measured. For convenience, we have also shown in Figure 14(b) the coverage area pattern corresponding to each placement configuration. We also show the line along which intensity has been calculated, appearing as a blue line crossing the coverage area. The transmitter and receiver parameters in this simulation are set based on available products. Existing LED light technology can emit energy ranging

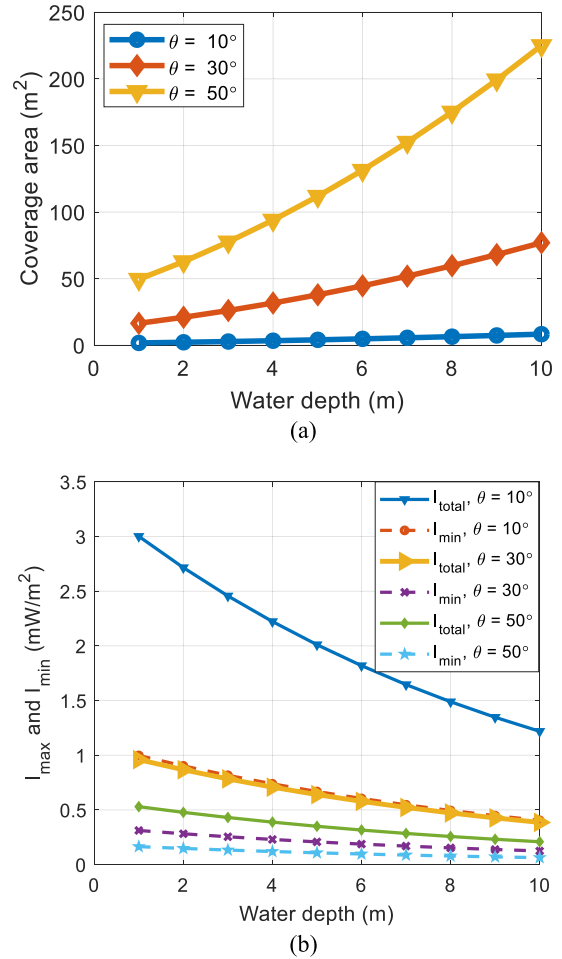


FIGURE 13. The effect of underwater distance on the coverage and light intensity for three collinear beamformed light sources places at height $d_a = 5m$ above the water surface.

from few mW to few Watts. For example, the DMX Wireless Transmitter/Receiver [36] can transmit up to 20 dBm (100 mW) light energy. Therefore, in this simulation, we have set the transmitted power, p , to 100 mW. In case of multiple light sources, we have distributed such power equally on all beamformed sources.

Figure 14 (I) shows the light intensity and coverage area for a single light source with $d_a = 10$ meters, $d_w = 25$ meters, $\theta = 10^\circ$ and $k = 0.4$. In Figure 14 (II), the values of d_a , d_w , and k stay the same except θ which is 20° in this case. Figures 14 (III) – (VI) show the simulation results for multiple light sources. All of the figures also depict the three threshold values of light intensities, marked by dotted lines. Each threshold reflects a setting for the minimum intensity required by a receiver for establishing a successful communication. The threshold value generally depends on receiver sensitivity, target Bit error rate (BER), and optical noise. The main sources of noise are ambient light, shot noise induced by the photodetector and electrical pre-amplifier noise which is also known as thermal noise [37]. In VLC, PIN photodiode and avalanche photodiode (APD) are the main types of receiver. Both of these receivers have sensitivity as low as

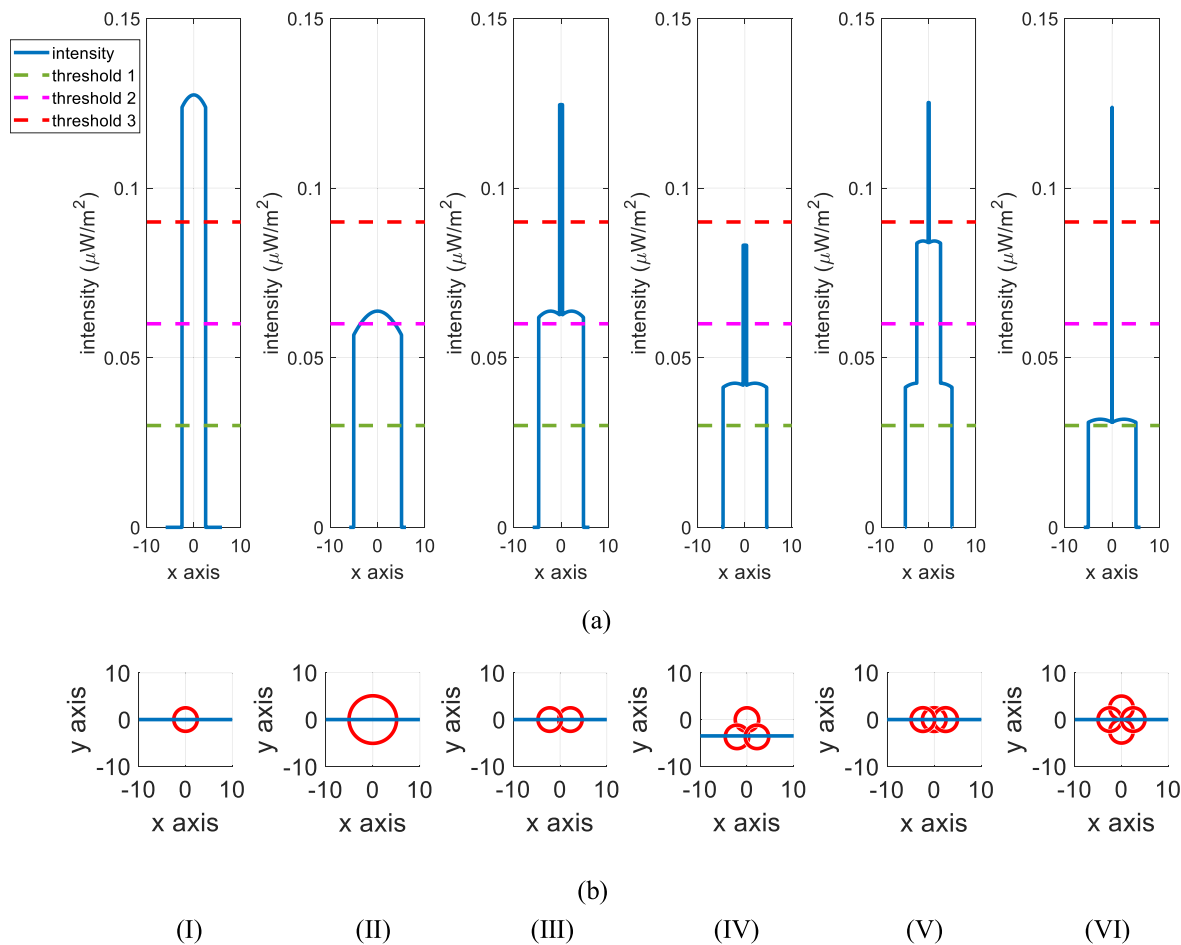


FIGURE 14. While assuming a flat water surface, a comparison of intensity and coverage area for a single light source with different beam angles in (I) and (II), and for beamformed sources in (III), (IV), (V), and (VI) where $d_a = 10$ meters and $d_w = 25$ meters.

few nW . Considering all of these factors, it was shown in [38] that the threshold value is -45 dBm ($0.03\mu W$) to achieve $BER = 1.5 \times 10^{-3}$ in absence of the ambient light. If we want to achieve lower BER we need to increase this threshold value.

In this simulation, we have considered threshold values of 0.03 , 0.06 and $0.09 \mu W$. From Figure 14(a), we can observe that for the first threshold setting, communication is possible for all single and multiple light sources arrangements except for the case of four light sources. If we use more than four light sources the scenario will be worse. Although a single light source with small beam angle (Figure 14 (I)) can achieve the threshold requirement, the coverage area is smaller than the arrangement shown in Figures 14 (II) – (V). Hence, in this case, the communication link is not robust, where robustness means the ability to cope with varying water conditions. Turbidity may increase the value of attenuation coefficient, k , and consequently diminishes the light intensity. In addition, the water current may drift away the underwater receiver from its position. Therefore, ensuring sufficient light intensity and large coverage area is important for link robustness. For the second threshold setting, only configurations (I) and (V) work and for threshold #3 only setup (I) allows

communication. Considering all three threshold settings, we can conclude that for high thresholds, a single light source with a small angle is preferable, though in this case coverage is not good. For low threshold values, a single light source with a relatively large beam angle can achieve enough intensity and coverage at the same time. However, for moderate threshold values employing three collinear light sources provides better coverage and intensity. Table 3 summarizes the above discussion.

B. WAVY SURFACES

Most of the time, the water surface is not flat where waves form due to the wind and earth gravity. We have used eq. (1) and eq. (4) to generate a wavy water surface. In this subsection, we discuss the simulation results for a wavy water surface for both single and multiple light sources.

A water surface wave has two important parameters, namely, wave amplitude and the time when the water surface function is captured. Such time can vary from 0 to the wave period, T . We have analyzed the effect of both parameters on the intensity when a single light source is used. In this simulation, the source is placed 5 meters above the water and the receiver is assumed to be at 5 meters depth, i.e., $d_a = 5$

TABLE 3. Coverage vs. intensity trade-off for different number of light sources where $d_a = 10$ meters and $d_w = 25$ meters.

No. of sources	Coverage (m^2)	I_{max} (μWm^{-2})	I_{min} (μWm^{-2})	Threshold (μWm^{-2})	Robustness	Communication
1($\theta = 10^\circ$)	19.88	0.13	0.12	threshold #1	low	yes
				threshold #2	low	yes
				threshold #3	low	yes
1($\theta = 20^\circ$)	80.23	0.063	0.056	threshold #1	high	yes
				threshold #2	no	no
				threshold #3	no	no
2	38.80	0.12	0.06	threshold #1	high	yes
				threshold #2	no	no
				threshold #3	no	no
3 (triangle)	57.58	0.08	0.04	threshold #1	no	yes
				threshold #2	no	no
				threshold #3	no	no
3(co-linear)	50.1	0.13	0.04	threshold #1	high	yes
				threshold #2	moderate	yes
				threshold #3	no	no
4	54.13	0.12	0.03	threshold #1	no	no
				threshold #2	no	no
				threshold #3	no	no

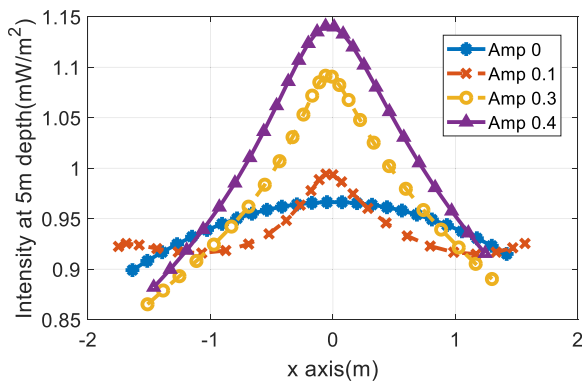


FIGURE 15. Effect of water surface wave’s amplitude on intensity for single light source.

meters and $d_w = 5$ meters. Figure 15 shows the results when the water wave’s amplitude is changed between, 0 (flat), 0.1, 0.3 and 0.4 meters. The plot reflects the intensity assuming a cnoidal shaped surface at zero time, i.e., the peak of the wave is vertically aligned with the light source. We can see intensity spreads almost equally within the coverage area for low amplitude, which means there is less deviation between the maximum and minimum intensity.

The water surface function always changes with time. Figure 16 shows the effect of time on light intensity when a single source is employed. The time can vary from 0 to wave period, T . Figure 16 shows the results for the time of 0, 0.5, and 0.8 sec, where the area covered by the light inside

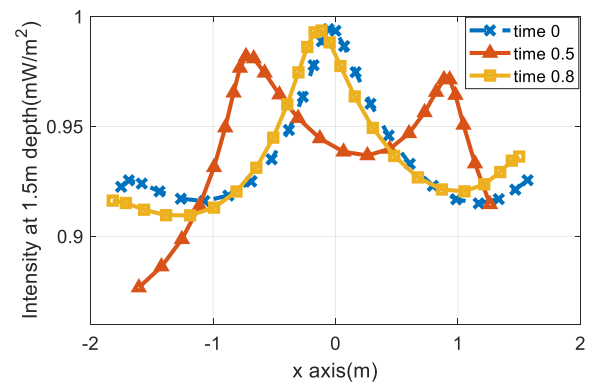


FIGURE 16. Effect of instantaneous time on intensity for single light source.

water always varies in accordance with time, as illustrated also in Figure 5.

The interest is in the effective coverage area which is covered by light all the time. Figure 17 shows the effective coverage area when applying Algorithm 1. For different θ ($\theta = 20^\circ, 30^\circ$, and 50°), Figures 17(a) and 17(b) provide the results for single and multiple light sources, respectively. When comparing Figures 17, 12(a) and 13(a), the effective coverage area is always smaller than the coverage area for a flat-water surface for both single and multiple light sources. Figure 18 shows the difference between coverage areas for single and multiple light sources for varying wave amplitude. Note that zero amplitude corresponds to a flat-water surface.

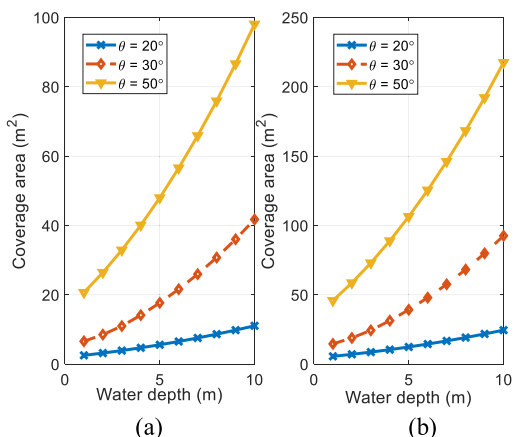


FIGURE 17. Coverage area in presence of water waves for both (a) single and (b) multiple light sources.

As evident from the figure, the coverage area diminishes with the increase of wave amplitude, which is expected given the increased scattering of light rays. Again, the use of multiple beamformed sources will yield better coverage; yet the effect of wave amplitude is consistent.

For multiple light sources, we have repeated the analysis of Figure 14 in presence of water waves. Again, we have considered the same parameters that we used for the flat water surface. Figure 19 shows the simulation results when the water wave’s amplitude equals 0.2 meter. The results are identical to those shown in Figure 14 except there are variations in the intensity between the maximum and minimum intensity due to the presence of surface waves.

C. LAB EXPERIMENTS

In order to validate the theoretical analysis and simulation results, a lab experiment has been conducted using

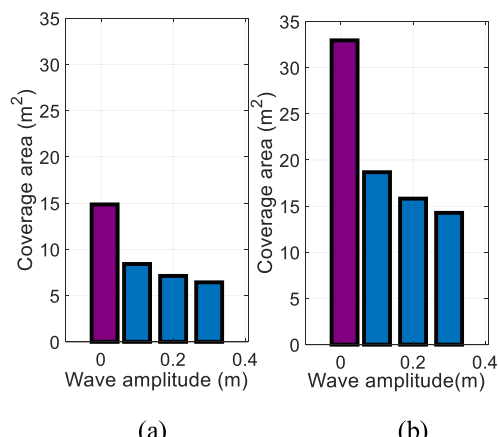


FIGURE 18. Changes in coverage area for different wave amplitude for (a) single light source and (b) three beamformed sources.

a 122 cm × 46 cm water tank. The tank is made of clear glass. Given the size constraint of the water tank, it is not possible to generate significantly-sized water waves that cause measurable impacts on the light intensity inside the water. Therefore, we conducted our lab experiment only for a flat-water surface. We have used blue LED light, which has the lowest attenuation coefficient in the water, as mentioned earlier. As a light source, we have used WAYLLSHINE® Zoomable Scalable CREE LED 3 Mode 200 Lumen 150 Yard Flashlight, which can be configured for different beam angles. As a photodetector 10mm² PIN detector (PC10-6b TO) has been used since it has a high response for blue LED light. In the experiment three light sources have been used with 10 mW power each. The water attenuation coefficient, *k* is measured and found to 0.1 m⁻¹. Due to the small room and tank size, the experiment is done with *d_a* = 0.25m and *d_w* = 0.46m. The beam angle is set to 52°, which is found to provide

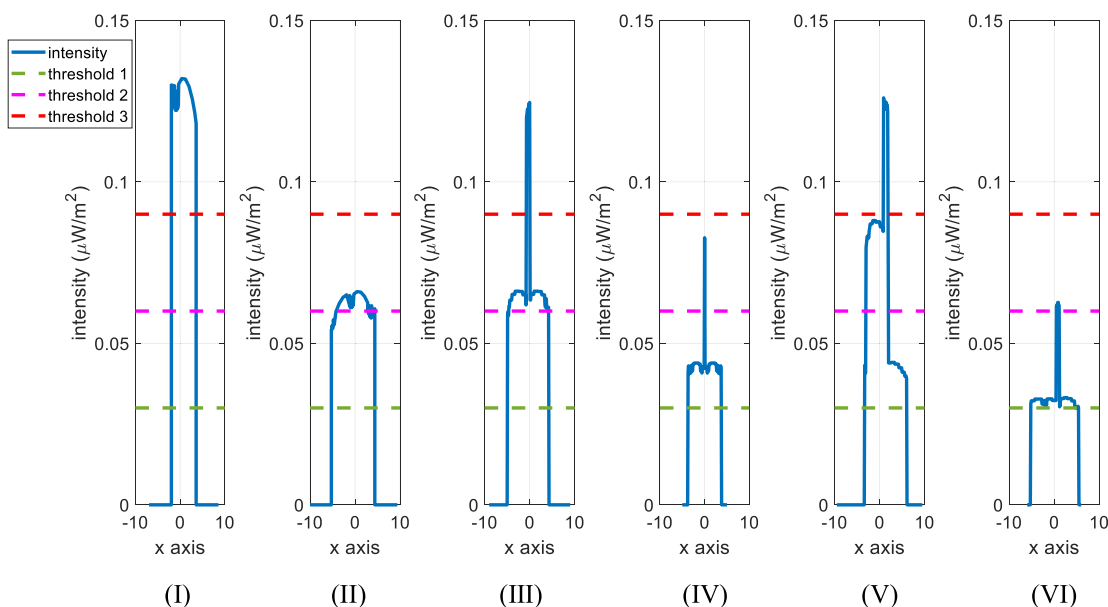


FIGURE 19. Comparison of intensity and coverage area for a single light source with different beam angles in (I), and (II), and for beamformed sources in (III), (IV), (V) and (VI), where *d_a* = 10 meters and *d_w* = 25 meters for a wavy surface.

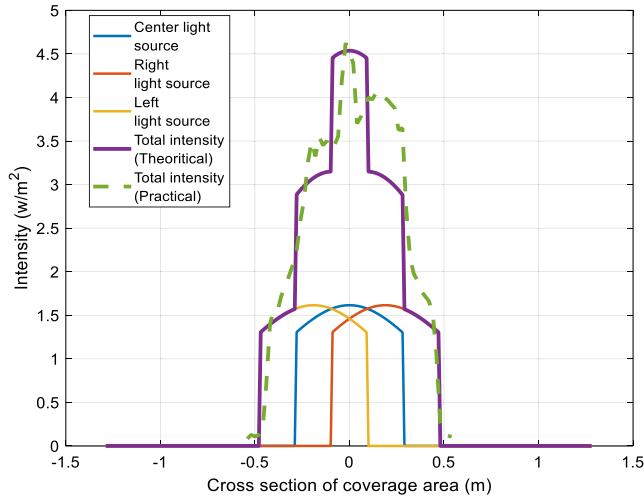


FIGURE 20. Experimental and theoretical results for light intensity at $d_a = 0.25\text{m}$ and $d_w = 0.46\text{m}$, with $\theta = 52^\circ$.

maximum coverage area inside the water tank for the above value of d_a and d_w . The experiment is done under dark setting to avoid the ambient noise from extremal light sources. Both the experimental and simulation result is shown in Figure 20. From this figure, we can see the experimental results almost match those obtained via simulation.

VII. CONCLUSION

The paper has studied the viability of establishing VLC links through the air-water interface in order to enable communication between an airborne base-station and underwater networks. Both the coverage area and light intensity have studied under flat and wavy water surface conditions. We first have considered a single light source and then extended the analysis for multiple beamformed light sources. In clean and steady water, a single light source provides better intensity. In the case of turbid water and/or wavy surface, we promote beamforming of multiple light sources which boosts coverage while keeping enough intensity for VLC communication. Coverage is very important in the presence of water current because an underwater node can drift away. The theoretical analysis has been confirmed by simulation and lab experiments.

APPENDIX A

CALCULATION OF WATER ATTENUATION COEFFICIENT

Using Beer’s law, we can find the attenuation of optical signal at distance d as follows [30]:

$$I = I_0 \cdot e^{-k(\lambda)d}, \tag{33}$$

where $k(\lambda)$ is the attenuation coefficient (m^{-1}) of water which is sum of absorption, a (m^{-1}) and scattering, b (m^{-1}) coefficient

$$k(\lambda) = a(\lambda) + b(\lambda). \tag{34}$$

The value of a and b depends on the biological factors of water and optical signal wavelength, λ . The absorption occurs mainly due to the pure water, chlorophyll-a, and humic and

fulvic acids. The expression to get the value of a can be described as [31], [32]:

$$a(\lambda) = a_w(\lambda) + a_f^0 C_f e^{-(k_f \lambda)} + a_h^0 C_h e^{-(k_h \lambda)} + a_c^0(\lambda) \left(\frac{C_c}{C_c^0} \right)^{0.602}, \tag{35}$$

where,

- a_w = pure water absorption coefficient (m^{-1});
- a_f^0 = specific absorption coefficient of fulvic acid;
- a_h^0 = specific absorption coefficient of humic acid;
- a_c^0 = specific absorption coefficient of chlorophyll in m^{-1} ;
- C_f = concentration of fulvic acid in mg/m^3 ;
- C_h = concentration of humic acid in mg/m^3 ;
- C_c = concentration of chlorophyll-a in mg/m^3 ;
- k_f = fulvic acid exponential coefficient, and
- k_h = humic acid exponential coefficient.

The scattering is mainly caused by the water and particles, and can be express as [31], [32]:

$$b(\lambda) = b_w(\lambda) + b_s^0(\lambda) C_s + b_l^0(\lambda) C_l, \tag{36}$$

where,

- b_w = water scattering coefficient in m^{-1} ;
- b_s^0 = scattering coefficient for small particulate matter in m^2/g ;
- b_l^0 = scattering coefficient for large particulate matter in cm^2/g ;
- C_s = concentration of small particles in g/m^3 , and
- C_l = concentration of large particles in g/m^3 .

The scattering albedo is defined as the ratio of the amount of scattering to the overall attenuation, i.e., $w_0 = \frac{b}{k}$. Eq. (33) is valid when there is no contribution of the scattering light in the received light. However, in turbid water scattered light may reentered in the receiver field of view (FOV). In that case we need to rewrite eq. (33) as follows [30]:

$$I = I_0 \cdot e^{-\gamma d}, \tag{37}$$

where

$$\gamma = a + (1 - n)b. \tag{38}$$

The scattering factor n ($0 \leq n \leq 1$) is used to recollect scattered light.

REFERENCES

- [1] D. Pompili and I. F. Akyildiz, “Overview of networking Protocols for underwater wireless communications,” *IEEE Commun. Mag.*, vol. 47, no. 1, pp. 97–102, Jan. 2009.
- [2] M. V. Jamali, A. Chizari, and J. A. Salehi, “Performance analysis of multi-hop underwater wireless optical communication systems,” *IEEE Photon. Technol. Lett.*, vol. 29, no. 5, pp. 462–465, Mar. 1, 2017.
- [3] M. S. Islam, M. Younis, and A. Ahmed, “Communication through air water interface using multiple light sources,” in *Proc. IEEE Int. Conf. Commun. (ICC)*, Kansas City, MO, USA, May 2018, pp. 1–6.
- [4] G. F. Edelmann, T. Akal, W. S. Hodgkiss, S. Kim, W. A. Kuperman, and H. C. Song, “An initial demonstration of underwater acoustic communication using time reversal,” *IEEE J. Ocean. Eng.*, vol. 27, no. 3, pp. 602–609, Jul. 2002.
- [5] S. Sendra, J. Lloret, J. M. Jimenez, and L. Parra, “Underwater acoustic modems,” *IEEE Sensors J.*, vol. 16, no. 11, pp. 4063–4071, Jun. 2016.

- [6] X. Che, I. Wells, G. Dickers, P. Kear, and X. Gong, "Re-evaluation of RF electromagnetic communication in underwater sensor networks," *IEEE Commun. Mag.*, vol. 48, no. 12, pp. 143–151, Dec. 2010.
- [7] L. Liu, S. Zhou, and J.-H. Cui, "Prospects and problems of wireless communication for underwater sensor networks," *Wiley Wireless Commun. Mobile Comput.*, vol. 8, no. 8, pp. 977–994, Oct. 2008.
- [8] I. F. Akyildiz, P. Wang, and Z. Sun, "Realizing underwater communication through magnetic induction," *IEEE Commun. Mag.*, vol. 53, no. 11, pp. 42–48, Nov. 2015.
- [9] M. C. Domingo, "Magnetic induction for underwater wireless communication networks," *IEEE Trans. Antennas Propag.*, vol. 60, no. 6, pp. 2929–2939, Jun. 2012.
- [10] J. W. Giles and I. N. Bankman, "Underwater optical communications systems. Part 2: Basic design considerations," in *Proc. IEEE Military Commun. Conf.*, Atlantic City, NJ, USA, Oct. 2005, pp. 1700–1705.
- [11] B. Cochenour, L. Mullen, A. Laux, and T. Curran, "Effects of multiple scattering on the implementation of an underwater wireless optical communications link," in *Proc. OCEANS*, Boston, MA, USA, Sep. 2006, pp. 1–6.
- [12] N. Farr, A. Chave, L. Freitag, J. Preisig, S. White, D. Yoerger, and P. Titterton, "Optical modem technology for seafloor observatories," in *Proc. OCEANS*, Boston, MA, USA, Sep. 2006, pp. 1–6.
- [13] T. Komine and M. Nakagawa, "Fundamental analysis for visible-light communication system using LED lights," *IEEE Trans. Consum. Electron.*, vol. 50, no. 1, pp. 100–107, Feb. 2004.
- [14] A. H. Azhar, T.-A. Tran, and D. O'Brien, "A gigabit/s indoor wireless transmission using MIMO-OFDM visible-light communications," *IEEE Photon. Technol. Lett.*, vol. 25, no. 2, pp. 171–174, Jan. 15, 2013.
- [15] F. Tonolini and F. Adib, "Networking across boundaries: Enabling wireless communication through the water-air interface," in *Proc. SIGCOMM*, Budapest, Hungary, Aug. 2018, pp. 117–131.
- [16] F. Blackmon and L. Antonelli, "Remote, aerial, trans-layer, linear and non-linear downlink underwater acoustic communication," in *Proc. OCEANS*, Boston, MA, USA, Sep. 2006, pp. 1–7.
- [17] X. Cheng, H. Zheng, and C. Yan, "BER evaluation and waveform analysis of nonlinear opto-acoustic communication system," *Optik*, vol. 124, no. 15, pp. 2000–2003, Aug. 2013.
- [18] X. Peng, W. Xu, X. Jin, and J. Shang, "Adaptive filter design for suppressing the moving surface interferences in opto-acoustic remote sensing," in *Proc. MTS/IEEE OCEANS*, San Diego, CA, USA, Sep. 2013, pp. 1–6.
- [19] H. C. Dy and R. C. Gustilo, "Characterization of signal response for surface water movements in underwater optical wireless communications," in *Proc. TENCON IEEE Region Conf.*, Cebu, Philippines, Nov. 2012, pp. 1–6.
- [20] M. V. Jamali, J. A. Salehi, and F. Akhondi, "Performance studies of underwater wireless optical communication systems with spatial diversity: MIMO scheme," *IEEE Trans. Commun.*, vol. 65, no. 3, pp. 1176–1192, Mar. 2017.
- [21] T. Sawa, N. Nishimura, and S. Ito, "Wireless optical Ethernet modem for underwater vehicles," in *Proc. 15th IEEE Annu. Consum. Commun. Netw. Conf.*, Las Vegas, NV, USA, Jan. 2018, pp. 1–4.
- [22] H. M. Oubei, C. Li, K. H. Park, T. K. Ng, M. S. Alouini, and B. S. Ooi, "2.3 Gbit/s underwater wireless optical communications using directly modulated 520 nm laser diode," *Opt. Exp.*, vol. 23, no. 16, pp. 20743–20748, 2015.
- [23] *LED Transmitter*. Accessed: Nov. 2018. [Online]. Available: <https://www.amazon.com/WAYLLSHINE-Zoomable-Scalable-Flashlight-Tactical/dp/B00W5PCTPW>
- [24] J. Sticklus, P. A. Hoehner, and R. Röttgers, "Optical underwater communication: The potential of using converted green LEDs in coastal waters," *IEEE J. Ocean. Eng.*, vol. 44, no. 2, pp. 535–547, Apr. 2019.
- [25] H. Brundage, "Designing a wireless underwater optical communication system," M.S. Thesis, Dept. Mech. Eng., Massachusetts Inst. Technol., Cambridge, MA, USA, 2010.
- [26] E. Infeld, A. Karczewska, and P. Rozmej, "Solutions to the extended KdV equation for water surface waves," *Nonlinear Dyn.*, vol. 91, no. 2, pp. 1085–1093, Jan. 2018.
- [27] M. W. Dingemans, *Water Wave Propagation Over Uneven Bottoms*. Singapore: World Scientific, Jan. 1997, pp. 708–715.
- [28] R. Wiegel, "A presentation of cnoidal wave theory for practical application," *J. Fluid Mech.*, vol. 7, no. 2, pp. 273–286, Feb. 1960.
- [29] M. Davies and A. K. Chattopadhyay, "Stokes waves revisited: Exact solutions in the asymptotic limit," *Eur. Phys. J. Plus.*, vol. 131, p. 69, Mar. 2016. doi: 10.1140/epjp/i2016-16069-7.
- [30] B. Cochenour, L. Mullen, and J. Muth, "Effect of scattering albedo on attenuation and polarization of light underwater," *Opt. Lett.*, vol. 35, no. 12, pp. 2088–2090, 2010.
- [31] L. J. Johnson, R. J. Green, and M. S. Leeson, "Underwater optical wireless communications: Depth dependent variations in attenuation," *Appl. Opt.*, vol. 52, no. 33, pp. 7867–7873, 2013.
- [32] V. I. Haltrin, "Chlorophyll-based model of seawater optical properties," *Appl. Opt.*, vol. 38, no. 33, pp. 6826–6832, 1999.
- [33] A. Mostafa and L. Lampe, "Optimal and robust beamforming for secure transmission in MISO visible-light communication links," *IEEE Trans. Signal Process.*, vol. 64, no. 24, pp. 6501–6516, Dec. 2016.
- [34] Y. S. Eroglu, A. Sahin, I. Guvenc, N. Pala, and M. Yuksel, "Multi-element transmitter design and performance evaluation for visible light communication," in *Proc. IEEE Globecom Workshops*, San Diego, CA, USA, Dec. 2015, pp. 1–6.
- [35] B. Wang, "Coverage problems in sensor networks: A survey," *ACM Comput. Surv.*, vol. 43, no. 4, Oct. 2011. Art. no. 32.
- [36] *DMX Wireless Transmitter/Receiver*. Accessed: Jul. 2019. [Online]. Available: <https://www.dioleed.com/custom/download/productFile/filename/DI-WLDMX-Specification%20Sheet.pdf/>
- [37] P. H. Pathak, X. Feng, P. Hu, and P. Mohapatra, "Visible light communication, networking, and sensing: A survey, potential and challenges," *IEEE Commun. Surveys Tuts.*, vol. 17, no. 4, pp. 2047–2077, 4th Quart., 2015.
- [38] G. Cossu, R. Corsini, A. M. Khalid, S. Balestrino, A. Coppelli, A. Caiti, and E. Ciaramella, "Experimental demonstration of high speed underwater visible light communications," in *Proc. 2nd Int. Workshop Opt. Wireless Commun. (IWOW)*, Oct. 2013, pp. 11–15.



MD SHAFIQUK ISLAM was born in Manikganj, Bangladesh, in 1990. He received the B.Sc. and M.Sc. degrees in applied physics, electronics, and communication engineering from the University of Dhaka, and the M.S. degree in computer engineering from the University of Maryland, Baltimore County, where he is currently pursuing the Ph.D. degree.

In 2015, he was a Lecturer with the Electrical and Electronics Engineering Department, Hamdard University, Bangladesh. Since 2015, he has been a Teaching Assistant with the Computer Science and Electrical Engineering Department, University of Maryland, Baltimore County (UMBC). He is also a Research Assistant with the Embedded Systems and Networks Laboratory, UMBC. His research interests include underwater optical communication, visible light communication, wireless sensor networks, and RF communication.



MOHAMED F. YOUNIS received the Ph.D. degree in computer science from the New Jersey Institute of Technology, USA. He is currently a Professor with the Department of Computer Science and Electrical Engineering, University of Maryland, Baltimore County (UMBC).

Before joining the UMBC, he was with the Advanced Systems Technology Group, Aerospace Electronic Systems Research and Development Organization of Honeywell International Inc. While at Honeywell International Inc., he led multiple projects for building integrated fault tolerant avionics and dependable computing infrastructure. He has also participated in the development of the redundancy management system, which is a key component of the Vehicle and Mission Computer for NASA's X-33 Space Launch Vehicle. He has published over 260 technical articles in refereed conferences and journals. He holds seven granted and three pending patents. His research interests include network architectures and protocols, wireless sensor networks, embedded systems, fault tolerant computing, secure communication, and distributed real-time systems. In addition, he serves/served on the Editorial Board for multiple journals and the organizing and technical program committees of numerous conferences. He is a Senior Member of the IEEE Communications Society.

...